Atmospheric Research 290 (2023) 106784

Contents lists available at ScienceDirect

Atmospheric Research

journal homepage: www.elsevier.com/locate/atmosres

Exploring severe weather environments using CM1 simulations: The 29 August 2020 event in the Balearic Islands

M. Vich *, R. Romero

Grup de Meteorologia, Departament de Física, Universitat de les Illes Balears, Ctra. de Valldemossa, km 7.5, Palma de Mallorca 07122, Illes Balears, Spain

ARTICLE INFO

Keywords:
Supercell storm
Severe weather
Heavy precipitation
CM1 simulations
Mesoscale ingredients
Western Mediterranean

ABSTRACT

On the morning of 29 August 2020, a supercell developed to the west of Mallorca (Balearic Islands, Spain) and then crossed the island. The storm produced strong winds, at least one EF2 category tornado on the Enhanced Fujita scale, heavy precipitation and large hail. The affected areas suffered power and landline phones outages, massive falling of trees that caused the closure of roads, and material damages on properties and infrastructures. Unfortunately this kind of high impact events are quite common in the western Mediterranean, specially during or near autumn, but generally elude the capabilities of standard forecasting procedures. A better understanding of their development and any improvement in their prediction are crucial to issue better warnings to civil protection and the general public.

Assessment of the Convective Available Potential Energy and Storm Relative Helicity present in the prior environment highlights the area where the actual supercell developed. However, neither the severity of the convective system nor other important properties such as its trajectory, can be predicted by the classic analysis of larger scale ingredients. This paper proposes a novel approach to obtain this additional information by applying the CM1 model. This cloud-resolving model was developed precisely to study convective storms and therefore emerges as the ideal tool to provide clues on the likelihood of a supercell and its severity and trajectory.

Specifically, we test the systematic run of several CM1 simulations over the favorable area highlighted by the classic analysis and explore the convective structures that can develop and evolve in such environments. The results point out the ability of the CM1-based method to capture for the 29 August 2020 event the supercell formation, its trajectory and severity parameters. Therefore, a CM1-based strategy can provide useful details about eventual convective structures and their characteristics, allowing forecasters to issue better weather warnings at operational level.

1. Introduction

The western Mediterranean region is annually affected by high-impact weather events, especially in the late summer and autumn (Tudurí and Ramis, 1997). Among these high-impact weather episodes, some events reach severity in the form of extreme rainfall intensities, large hail, down-bursts and tornadoes. As a local example, statistics calculated from the 1989–1999 period tornado reports in the Balearic Islands show a total of 23 tornadoes recorded events, with 30% of the cases reaching F2 intensity in the Fujita scale (Gaya et al., 2001). A more modern and improved version of the original Fujita Scale, the Enhanced Fujita Scale, is now widely used world-wide (e.g SPC, 2007 or EC, 2013).

Convective systems that lead to severe events are common in the western Mediterranean. There are numerous documented events such as Ducrocq and Bougeault (1995), Ramis et al. (1997), Ramis et al. (1999) or Romero et al. (2015) that study squall lines, Homar et al. (2001) or Gayà (2011) that examine tornados or Sánchez et al. (2003) that investigate a hail event. In most of these events the severe convection developed and evolved over land, while in fewer events like that of 4 October 2007 in Mallorca (Ramis et al., 2009) the precursor processes occurred over maritime areas. In the event studied here, the severe supercell also developed and evolved over the sea until it reached land at the northwestern coast of Mallorca.

The aim of this work is to describe and analyze the severe convective environment that led to the 29 August 2020 supercell in Mallorca. The classic analysis of convective indices, like instability and helicity, is complemented with a novel approach based on application of the Cloud Model 1 (CM1; Bryan and Fritsch, 2002; Bryan, 2008b). This approach

* Corresponding author.
E-mail address: mar.vich@uib.es (M. Vich).

https://doi.org/10.1016/j.atmosres.2023.106784
Received 13 December 2022; Received in revised form 18 April 2023; Accepted 25 April 2023
Available online 3 May 2023

allows to obtain more detailed information regarding the characteristics and effects of the potential convective systems.

The CM1 model was designed primarily for idealized research, particularly for deep moist convection (i.e., thunderstorms), so it is a good tool to asses the convective potential of an environment. If fed with a pseudo-radiosounding that characterizes the basic state, a CM1 run provides detailed insight about the convective potential of the environment and on the likelihood of organized thunderstorms like multicells, squall lines or as in the present case study, supercells. The method also provides relevant information on the supercell properties, like severity and trajectory. This additional information can be very useful to asses the severity of a convective environment, specially in an operationally forecasting context where the forecaster needs to decide whether to issue a warning based on the available information beforehand.

The ability of the CM1 model to provide insights of convective structures has been proved in a wide range of earlier studies. For example, Spiridonov et al. (2021) analyse a supercell storm that occurred at the Vienna International Airport on 10 July 2017 and produced large hail and a F2 tornado. This study relies on WRF and CM1 models to examine the triggering factors of the supercell and posterior tornado formation and evolution; it also evaluated their location and intensity. The CM1 model is also used in Wade and Parker (2021) to simulate high-resolution supercells to investigate low-CAPE environments potential. All simulated storms present heavy precipitation and their reflectivity fields show classical supercell structures. Schueth et al. (2021) examine the reflectivity and winds obtained in a high-resolution tornadic supercell CM1 simulation to investigate the stream wise vorticity current. Patra et al. (2022) implement different stochastic parameterizations in the CM1 model to asses the sensitivity of tropical cyclone intensity (wind) to these random parameterizations. Another example is Boyer and Dahl (2020), that simulates several supercells and quasi-linear storms with the CM1 model to investigate the role of large near-surface vertical vorticity in their development.

The paper is structured as follows: Section 2 describes the event and presents a large scale analysis of severe convective ingredients; Section 3 details the methodology and results of our approach consisting of applying the CM1 model to analyze in detail the convective potential of the environment; finally Section 4 presents the main conclusions obtained in the study.

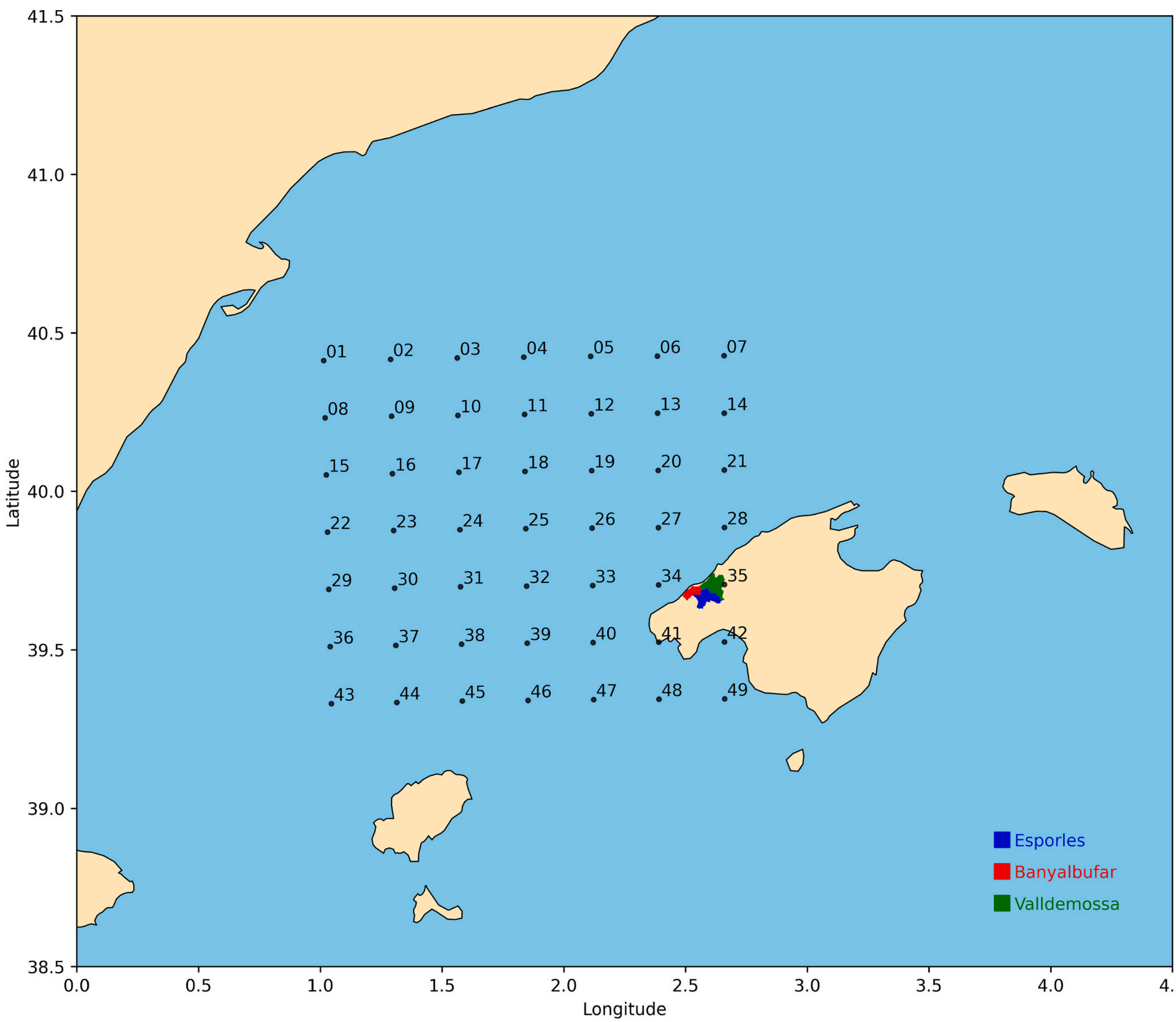

Fig. 1. Map of the Balearic Islands. The affected municipalities of Mallorca are highlighted in colors. The labeled dots show the location of the 49 pseudo-soundings used to initialize CM1 runs.

2. Description of the event and large scale analysis of the severe convective potential

On 29 August 2020, a supercell developed over sea to the west of the Balearic Islands (Spain). At around 11:30 local time (9:30 UTC) the associated storm reached the northwest coast of Mallorca and severely affected the municipalities of *Banyalbufar*, *Esporles* and *Valldemossa* of the *Serra de Tramuntana* (see Fig. 1). The storm produced several downbursts, at least one tornado, heavy precipitation and hail larger than 2 cm. The *Banyalbufar* meteorological station is the only AEMET station in the vicinity of the affected region (AEMET - Agencia Estatal de METeorología, the National Weather Service of Spain). According to its registers, the station experienced southwesterly winds with gusts reaching an exceptional speed of 171 km h^{-1}, which is a record value for this station. However, based on field analysis of the damage undertaken by government officials, it is estimated that the gusts would have reached values up to 190 km h^{-1}, corresponding to EF2 category winds in the Enhanced Fujita scale (winds between 179 and 218 km h^{-1}). In fact, the Environment and Territory Department of the Insular Government estimated that the wind uprooted most of the trees in 736 hectares of forest area, causing the closure of several roads and the interruption of electricity and telephone supplies in the affected municipalities, as well as material damages on properties and infrastructures (AEMET, 2020a, b).

The visual appearance of the convective cloud base as photographed from *Puig de la Moneda, Valldemossa* (Fig. 2) shows a distinctive greenish color along the horizon. This cloud tint is commonly observed in intense thunderstorms as the absorption of sunlight by rain and hail could lead to a green sky (Bohren and Fraser, 1993; Gallagher et al., 1996; Wang, 2002; Ramis et al., 2009; Romero et al., 2015).

Constant Altitude Plan Position Indicator (CAPPI) images at 2.5 km altitude from the radar at the Balearic Islands (Fig. 3) show a supercell formation occurring about 130 km to the west of Mallorca that splits at around 0630 UTC. The anticyclonic cell moves north–northeastwards while the cyclonic one points east-southeastwards. At around 0830 UTC the radar shows a hook-echo signature just off the Mallorcan coast. Precipitation intensity within the supercell was very important as indicated by reflectivity values reaching as high as 60–66 dBZ. By 0930 UTC a V-Notch structure is formed over the north of Mallorca, traveling eastwards. The supercell crossed Mallorca and continued towards the south of Menorca before dissipating at around 1230 UTC. This supercell lived more than 8 h according to the radar signal.

The large-scale meteorological environment in which the supercell developed was characterized, first of all, by a subtropical anticyclone located west of the Iberian Peninsula (see Fig. 4.a). A low-pressure system over the continent with its centre situated over the North Sea was driving a basic northerly flow over west Europe. However, a secondary low-pressure system located over the western Mediterranean was deflecting this general flow and advecting warm and moist maritime air towards the islands. The temperature field at 850 hPa shows a clear temperature gradient over the eastern part of the Iberian Peninsula associated with the cold front (Fig. 4.a). At mid-tropospheric levels, 500 hPa, Fig. 4.b shows a prominent trough with its axis extending along the Iberian peninsula. At 250 hPa, Fig. 4.c shows the wind speed and direction, clearly following the trough that guided the circulation. As the synoptic pattern evolved eastwards, this upper level jet entered over the western Mediterranean, favoring deep-layer shear in the Balearic Islands environment. The *Meteosat* images (see Fig. 5) show the cloudiness associated with the passage of the cold front, along with a more compact structure ahead of it that accompanies the supercell life cycle (see Fig. 3).

Once the large-scale meteorological environment of the event has been described, we focus on exploring the convective potential of the troposphere that allowed the supercell development. Specifically, the Convective Available Potential Energy (CAPE) and the Storm Relative Helicity (SRH) indices are assessed, as both are widely used by the community to this end (e.g. Meukaleuni et al., 2016; Coffer et al., 2019; SPC, 2022). Here, both indices are evaluated using the 00UTC 29 August 2020 meteorological forecast provided by the Global Forecast System (GFS) model maintained by the National Centers for Environmental Prediction (NCEP). One the one hand, Fig. 6.a shows how the CAPE structure moves from the north–northwest to the south-southeast, following the same direction as the cold front and the storm itself. Specifically, the region of the supercell generation (northwest of Mallorca Island) presents values of CAPE between 1000 and 2500 J kg^{-1} that suggest moderate-to-strong instability. Higher CAPE values are

Fig. 2. Photograph of the thunderstorm taken from Puig de la Moneda, Valldemossa, on 29 August 2020 at around 0900 UTC when it was about to reach the coast. Photograph kindly provided by Lluís Salvà Pou.

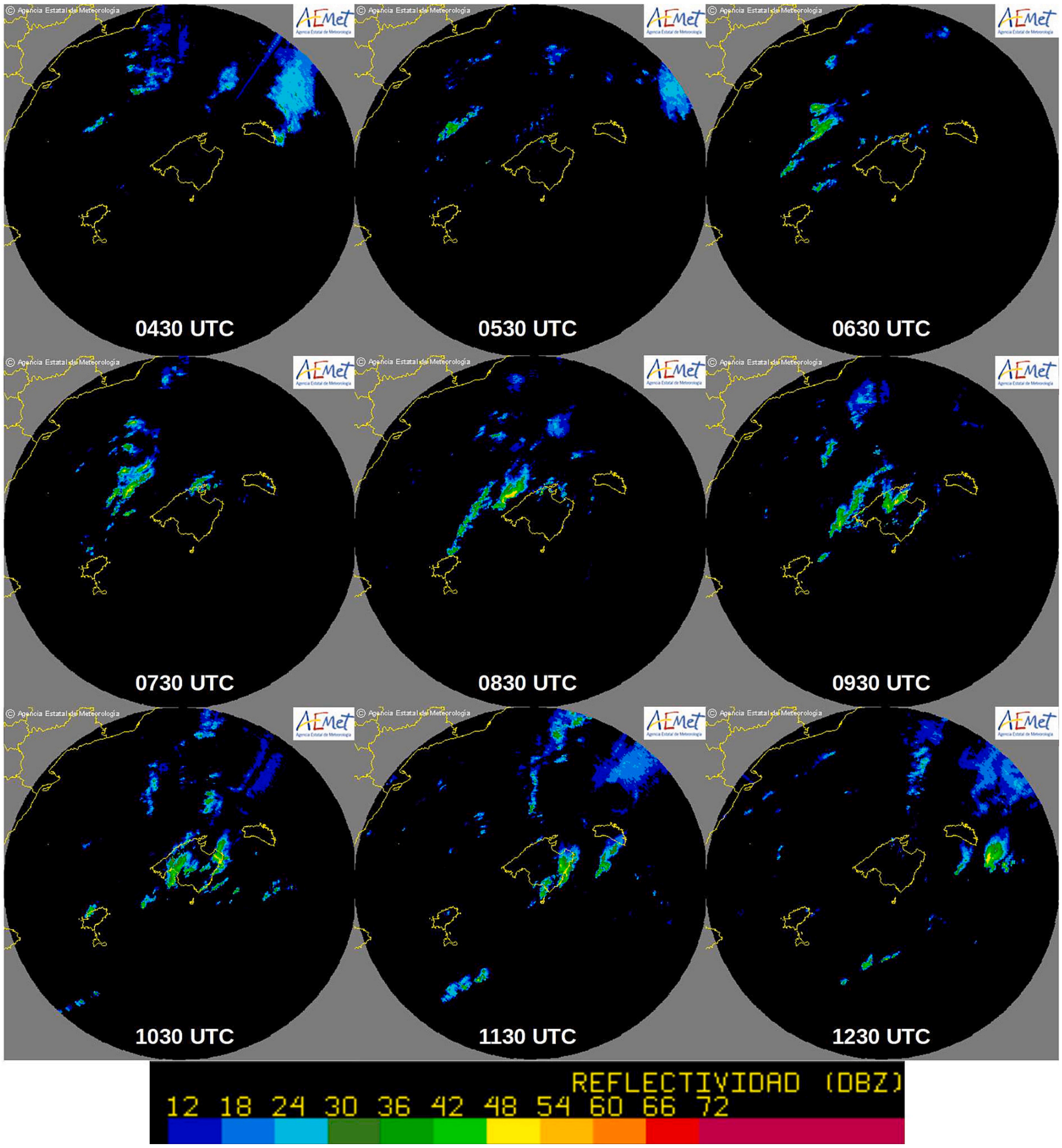

Fig. 3. Hourly series on 29 August 2020 of CAPPI images at 2.5 km altitude from the Mallorca radar.

found southeast of Mallorca that evidence the convective potential surrounding Mallorca during the episode. On the other hand, Fig. 6.b shows that SRH follows a similar geographical evolution of CAPE but shifted backwards. This SRH field refers to the 0–3 km layer and uses for the estimated storm movement the Internal Dynamics method developed in Bunkers et al. (2000). Also, values of SRH larger than 250 $m^2 s^{-2}$ are located again to the northwest of Mallorca Island. This threshold is significant because 0–3 km SRH values greater than 250 $m^2 s^{-2}$ suggest increased threat of tornadoes and supercells (SPC, 2022).

Both CAPE and the SRH indices can be combined to obtain the Energy Helicity Index (EHI; See Rasmussen (2003) and Hart and Korotky (1991) for more details). Specifically, the EHI is formulated as

$$EHI = \frac{SRH \cdot CAPE}{160000} \quad (1)$$

This index is revealed as a prominent indicator of tornadic potential since it relies on the idea that storm rotation should be maximized when instability (CAPE) and helicity (SRH) are both large (Hart and Korotky, 1991; Rasmussen, 2003; Thompson et al., 2003). Fig. 6.c highlights the fact that EHI is a combination of CAPE and SRH as its evolution follows the same north–northwest to south-southeast direction of both individual ingredients. However it moves slower -the EHI structure is almost stationary over the islands- as it maximizes in the front and rear, respectively, of the SRH and CAPE patterns. Regarding the EHI magnitude, values larger than 1 indicate supercell potential, while values between 1 and 5 suggest that EF2 and/or EF3 tornadoes are possible. Accordingly, Fig. 6.c clearly shows the accentuated potential for supercells all over the Balearic Islands and possible EF2 tornados in some regions, including the region where the supercell actually developed. As already stated, the recorded winds at the nearest meteorological station and the ground effects both confirm a EF2 category tornado in the region, whereas the radar images confirm the supercell signature during the event.

The analysis of the GFS forecasts fields puts forward the severe convective potential of the environment of 29 August 2020 that lead to the catastrophic winds, rain and hail on the northwest coast of Mallorca. However, although the convective potential is well captured in these forecast fields, and they are compatible with the actual outcome, they do not provide information on the probability of a supercell, the timing and location of its eventual formation, the maximum intensity the storm

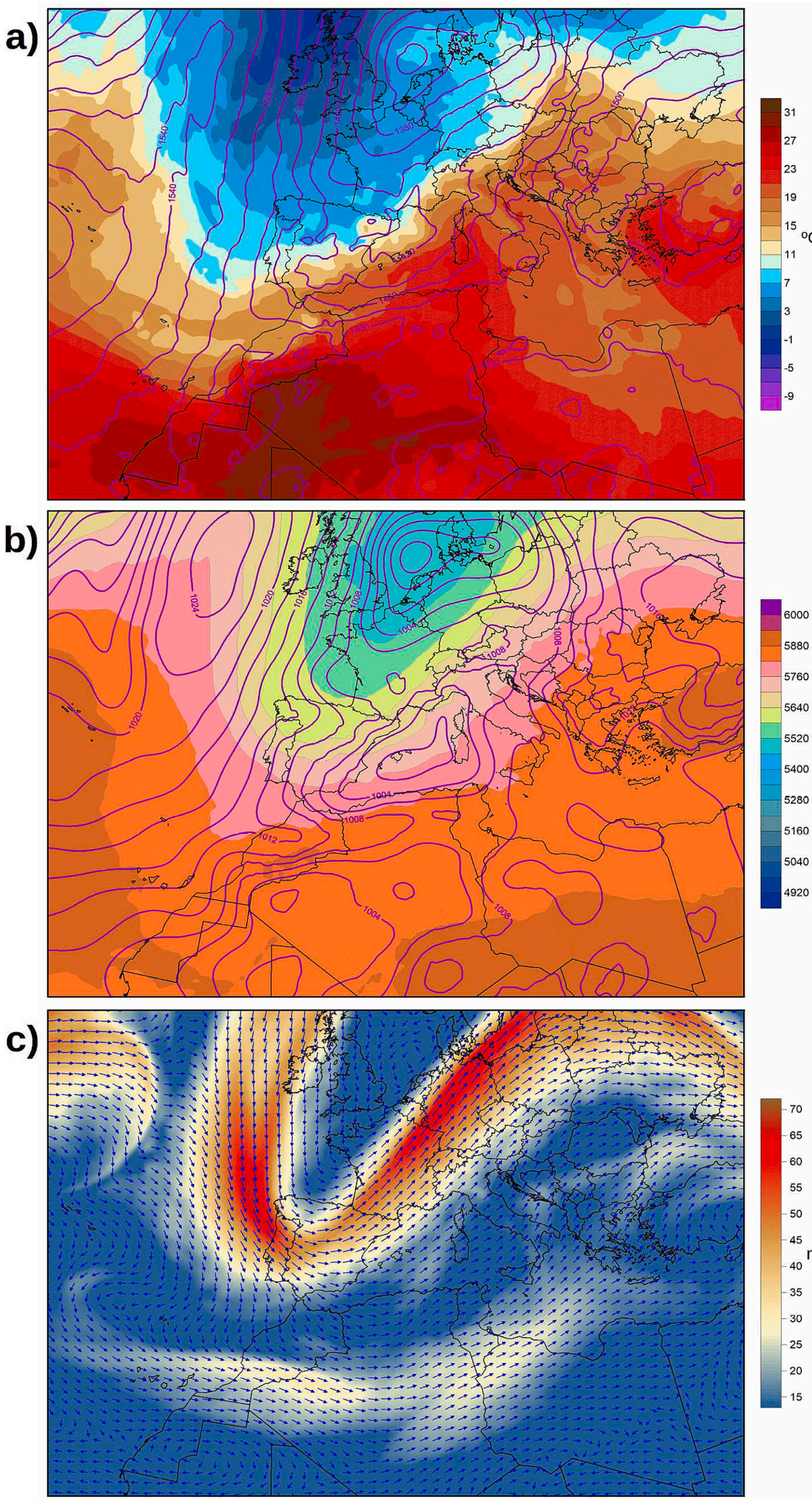

Fig. 4. Synoptic scale analysis from the GFS forecast on 29 August 2020 at 0000 UTC, valid at 0600 UTC. a) Geopotential height (solid line, in m) and temperature (colored field, in ºC) at 850 hPa; b) Mean Seal Level pressure (solid line, in hPa) and geopotential height at 500 hPa (colored field, in m); and c) Wind field at 250 hPa, the speed is represented in m s^{-1} according to the colored field and the direction is indicated with the arrows.

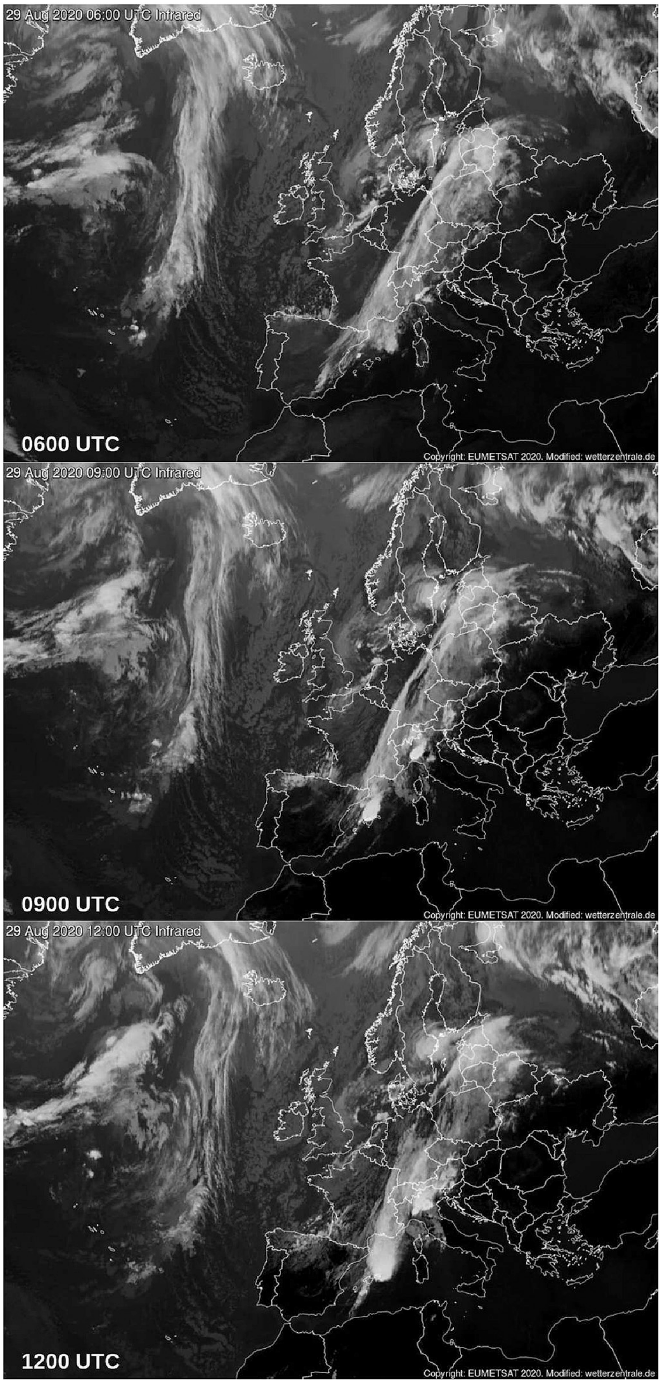

Fig. 5. IR *Meteosat* images on 29 August 2020. Images available at wetterzentrale.de - Copyright EUMETSAT 2020.

would attain and the expected effects in case it reached the coast. In the next section, an approach to improve the knowledge of these important details - prior to the actual event - will be presented and discussed.

3. CM1 based analysis of the severe convective environment

The CM1 model is a three-dimensional, nonhydrostatic, fully-compressible and time-dependent numerical model. It was designed for idealized studies of atmospheric phenomena driven by relatively small-scale processes, such as thunderstorms. It has been widely applied during the last decade in supercell and tornado research (e.g. Markowski and Dotzek, 2011; Markowski and Richardson, 2014; Orf et al., 2017; Peters et al., 2020; Jo and Lasher-Trapp, 2022). By design, the CM1 model is an ideal tool to explore the convective potential of an environment like the one present in the Balearics on 29 August 2020. In this section, we explore the application of several CM1 runs over the region highlighted by the classic severe convective potential parameters (CAPE, SRH and EHI) to obtain more details on the likelihood of a supercell and its characteristics.

3.1. Methodology

The CM1 version release 20.2 was used to perform all simulations. The model conserves mass and energy better than other modern cloud models (Bryan, 2008b). However, it is limited by its idealized convection initiation and by using an initially horizontally homogeneous environment as far as the simulation realism is concerned. Therefore, our approach relies on a set of idealized simulations using an observed proximity sounding to define the base state and a warm bubble to initiate convection.

The governing equations are the filtered Navier–Stokes equations (i.e., Large-Eddy Simulation equations; more details in Bryan, 2008b). Temporal advance is performed with the Runge–Kutta 3rd order scheme (Wicker and Skamarock, 2002). The Klemp-Wilhelmson time-splitting method for acoustic modes is used for the pressure solver, with a vertically implicit solver and horizontally explicit calculations, as in MM5 and WRF models (Dudhia, 1993; Skamarock et al., 2019). The advection terms are discretized using a fifth-order spatial discretization and no artificial diffusion is applied. The subgrid turbulence parameterization is similar to the parameterization of Deardorff (1980) that relies on turbulence kinetic energy (TKE). The microphysics parameterization includes five types of hydrometeors (cloud droplets, raindrops, ice, snow, and graupel) following the Morrison double-moment scheme (Morrison et al., 2005; Morrison et al., 2005), a realistic setup for a supercell simulation. No topography is considered in the simulations. The lateral boundary conditions are open radiative, while the bottom and top boundaries conditions are free-slip (no friction). No surface heat fluxes are imposed and Coriolis acceleration is not included either. The absence of terrain, surface heat fluxes, radiative forcing and Coriolis force allows the model basic environment to remain steady during the simulations (Markowski and Dotzek, 2011).

The horizontal grid spacing for the simulations is 1 km within a 120 km $\times$ 120 km region. The domain moves eastward with at a constant speed of 5 m s^{-1} to better follow the progression of the supercell when developed. The vertical grid spacing is 500 m within a 20 km vertical extent (i.e. 41 levels). A symmetric ellipsoidal warm bubble 10 km wide and 2.8 km deep is added in the initial field to provide a trigger for the supercell formation. Specifically, the maximum potential temperature perturbation is of 5 K at its center (located at 1.4 km above ground level, 60 km in the x-direction from the western boundary and 40 km in the y-direction from the southern boundary), and decreasing gradually to zero at its outer edge. The large time step of the model is set at 6 s. Each simulation runs for 3 h.

The environments of the simulations are initialized with a pseudo-sounding. The pseudo-soundings are derived from the 29 August 2020 00UTC GFS forecast runs valid at 03, 06 and 09 UTC. A vertical profile of the relevant variables (following the CM1 criteria on how to construct the input sounding file; Bryan, 2008a) is extracted from the GFS forecast field at the geographical location of interest. However, the available GFS forecast fields only include 31 standard pressure levels, largely omitting the structure of the atmospheric boundary layer. It is well known that the vertical resolution is an important limiting factor when considering convective inhibition and initialization (see for example Taszarek et al., 2021; Weisman and Klemp, 1982). In order to produce a proper vertical structure of the meteorological fields, an extra step to enhance the pseudo-sounding is performed. These improved pseudo-soundings are generated by exposing the GFS forecast fields as input fields for a 1-h run with the Triangle-based Regional Atmospheric Model, a nonhydrostatic,

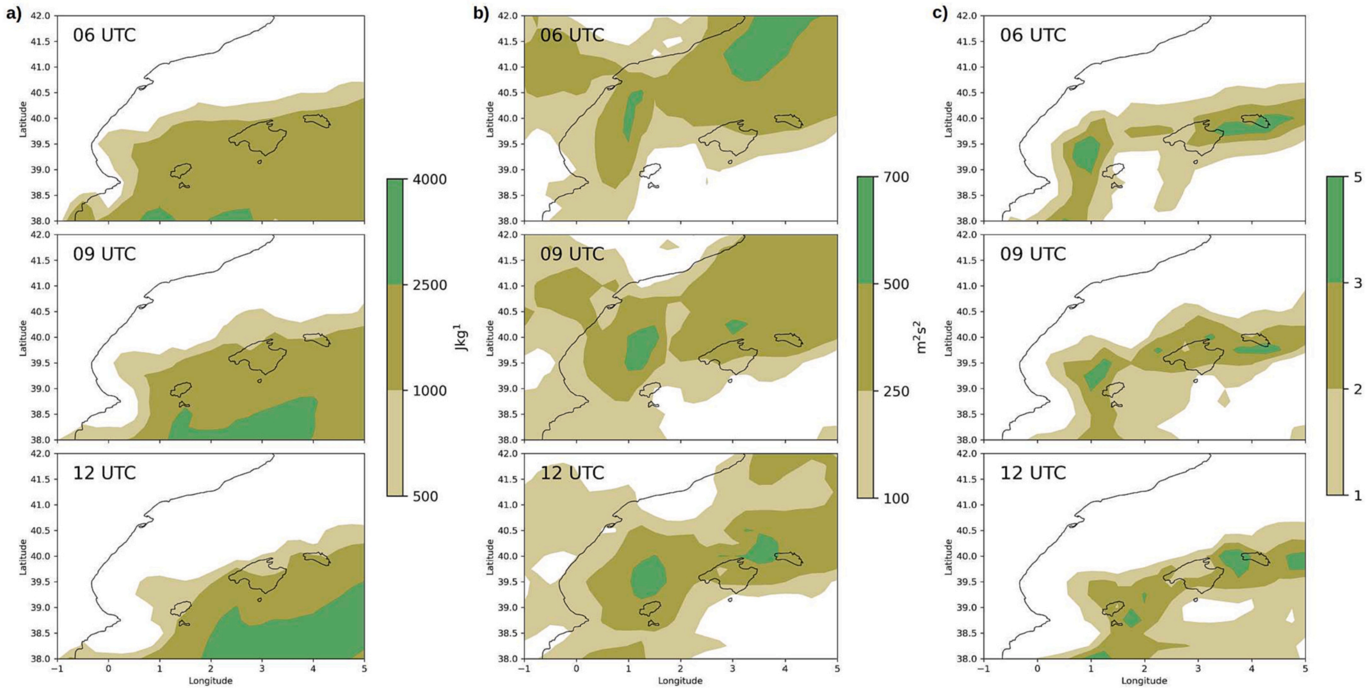

Fig. 6. From the GFS forecast of 29 August 2020 issued at 00 UTC, corresponding to 06, 09 and 12 UTC (from top to bottom, respectively): a) Convective Available Potential Energy (CAPE) for the most unstable parcel in the lowest 180 mb, b) Storm Relative Helicity (SRH) in the layer 0–3 km and c) Energy Helicity Index (EHI).

fully compressible numerical model (TRAM; Romero et al., 2019). These 1 h-runs with TRAM allows to increase the vertical levels from 31 to 52, with enhanced resolution in the planetary boundary layer (PBL). The short duration of the TRAM model run allow to properly balance the meteorological fields in the vertical, effectively accounting for the turbulence mixing, while avoiding relevant model dependent dynamics of regional or convective scale. The TRAM configuration is the same as in the operational run of finest resolution (approximately 2 km x 2 km) launched twice daily over the Balearics by the UIB Meteorology Group (TRAM SR; see Romero, 2020).

Fig. 1 shows the location of the 49 TRAM SR grid points where the vertical profiles are extracted to build the improved pseudo-soundings, subsequently ingested in the CM1 runs. These 49 locations form a 7x7 points square centered to the northwest of Mallorca, covering the region highlighted by the CAPE, SRH and EHI ingredients and where the supercell of 29 August 2020 evolved.

3.2. Results

In this section, the results of the proposed 49 simulations are examined. We focus on the outputs concerning the convective potential, thunderstorm organization and degree of severity allowed by the basic environment at their respective geographical locations.

Fig. 7 shows the maximum reflectivity in the atmospheric column at the beginning, middle and end of the simulated period (30, 100 and 180 min, respectively) for the experiments initialized at 03 UTC 29 August 2020. The simulations are examined in terms of the location of their pseudo-soundings with respect to the southwest-northeast diagonal of the diagram (almost parallel to the coast of Mallorca) and with respect to its distance to the bottom-right corner (covering part of Mallorca, including the affected area; see Fig. 1 for reference). At the beginning of the simulation the runs near the diagonal, specially those close to the northeast corner, develop convective storms with up to 60 dBZ signals of maximum reflectivity. However, these convective structures are short-lived and dissipate quickly, even before the 100 min simulation time.

Equivalent examination of the runs initialized at 06 UTC (Fig. 8) show that more members than three hours earlier develop big convective storms. This happens now at both sides of the diagonal. These more robust thunderstorms are long-lived and most of them survive until the end of the simulation. Many of these convective systems show a storm-splitting behaviour similar to the splitting of the observed supercell, with a preponderance of the right mover cell towards the end of the simulated period. Their associated values of maximum reflectivity attain 70 dBZ.

Finally, the runs initialized at 09 UTC (Fig. 9) develop convective systems at almost all locations at the beginning, but only those located towards the southeast corner (i.e. environments close to Mallorca) survive until later stages of the simulation. These runs exhibit again a storm-splitting behaviour similar to the splitting of the observed supercell and values of composite reflectivity up to 70 dBZ.

We seek a method to summarize the above results for the maximum reflectivity and other fields of interest. We compute at each analysed time step the maximum spatial value of the variable of interest for each one of the 49 CM1 maps. The result is then represented according to a color scale on a 7 x 7 pixel image corresponding to the original geographic location of the CM1 runs.

Fig. 10 shows these computed values for the maximum reflectivity of the CM1 runs initialized at 03, 06 and 09 UTC. In agreement with Figs. 7–9, Fig. 10 highlights the fact that the convective structures develop near the northwest corner for the 03 UTC runs, while their development shifts to the diagonal region in the 06 UTC runs and continues to move to the southeast corner in the 09 UTC runs. This southeastwards displacement of effective environments for the triggering and maturation of intense storms as the runs are initialized at later times, agrees with the evolution of the synoptic situation (recall Section 2). However, differences appear between the different initialization times. The convection developed in the 03 UTC runs decays quickly and does not persist across the southwest-northeast diagonal. In the 06 UTC runs, the convective storms develop on both sides of the diagonal and, as simulation time advances, they are also favoured near and over the coast of Mallorca. The convective structures in the 09 UTC runs are already well developed for the environments at the end of the simulations taken from the southeast quadrant (Mallorca).

The evolution of deep convection signatures in each run is in

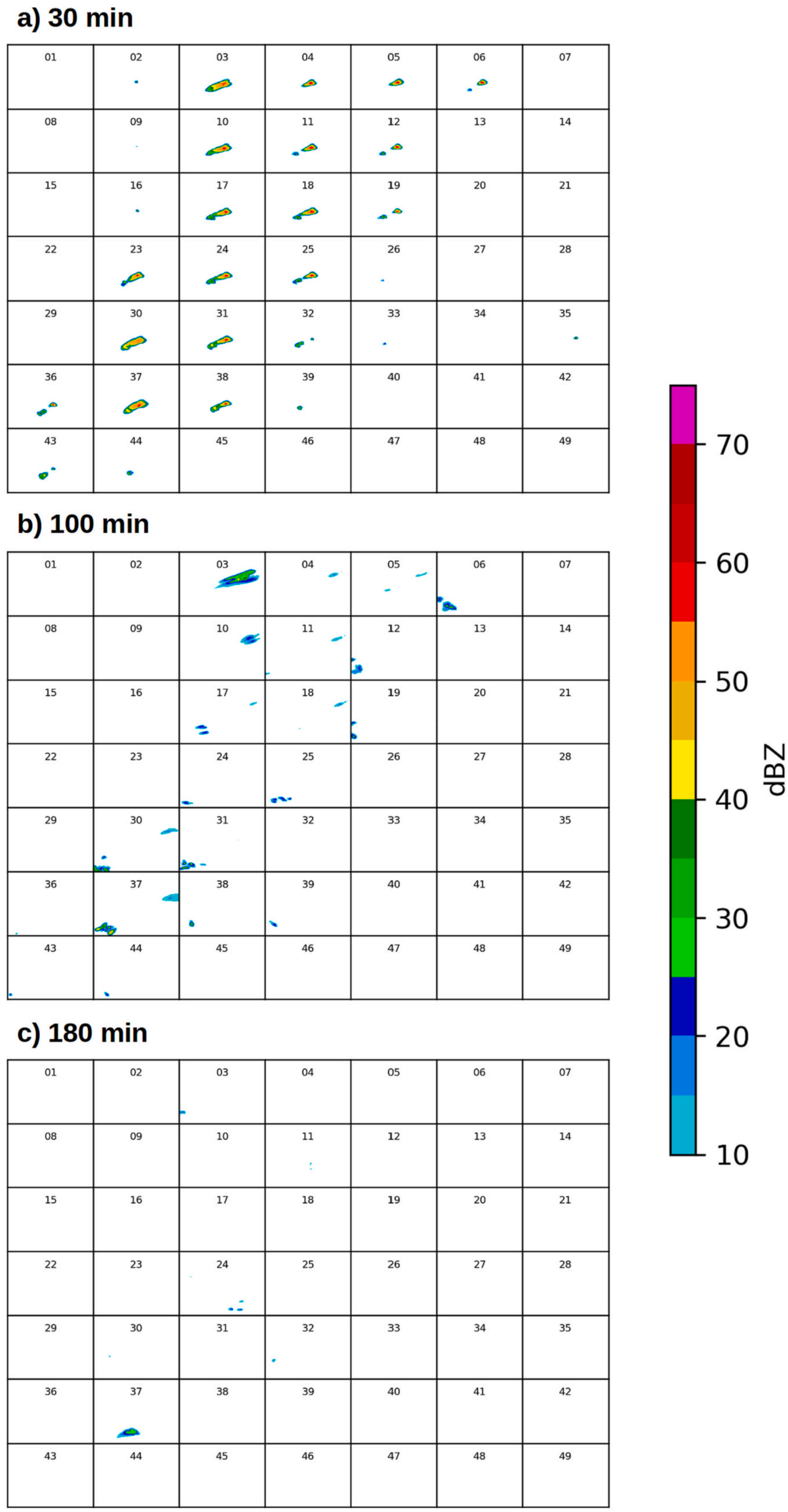

Fig. 7. The 30, 100 and 180 min simulation time output for the Maximum Reflectivity (dBZ) from the 49 CM1 simulations initialized with the 03UTC 29 August 2020 00UTC GFS forecast fields. The 49 simulation maps are placed following the 7 points x 7 points initial soundings presented in Fig. 1.

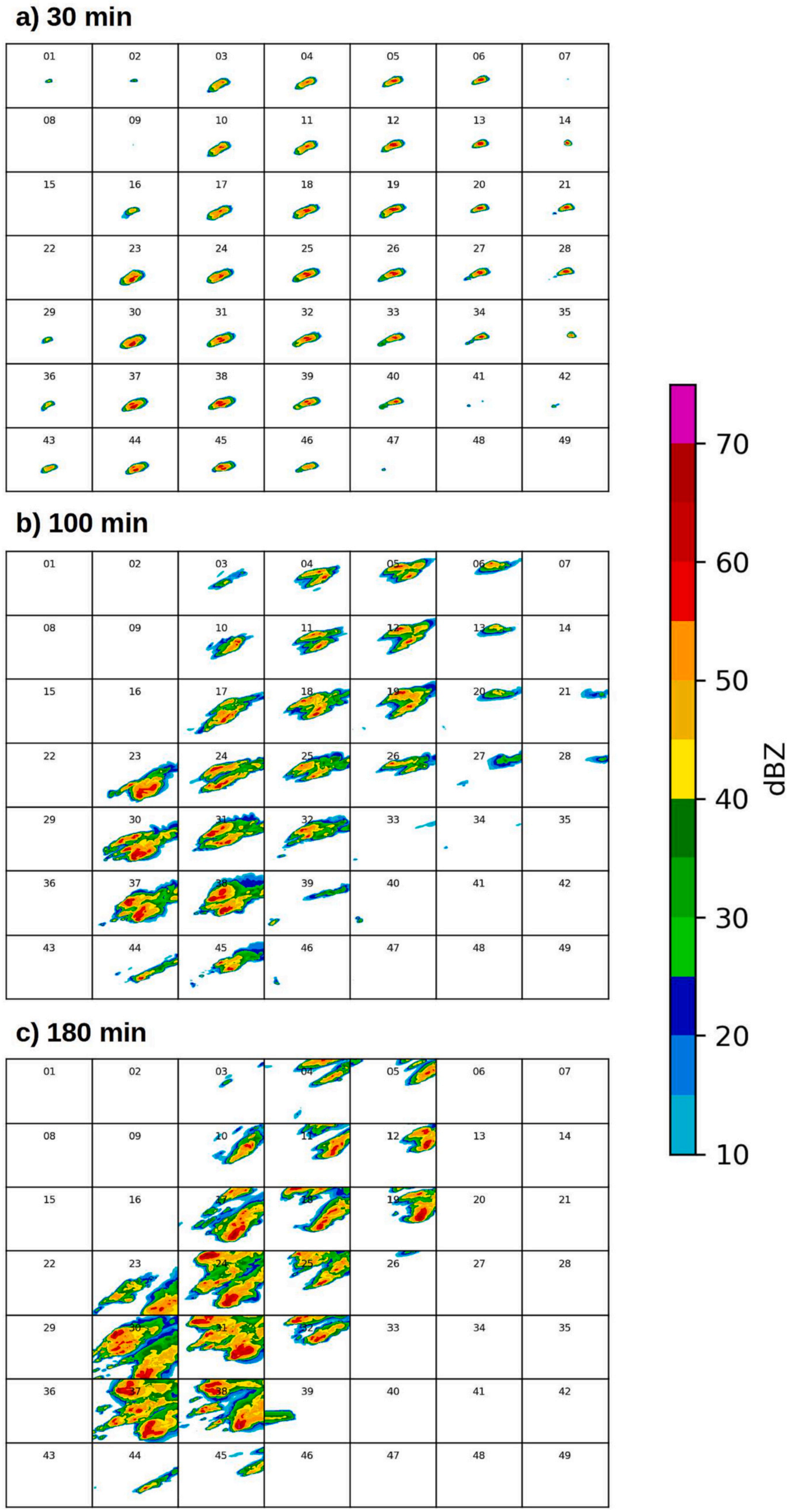

Fig. 8. As in Fig. 8 but for the simulations initialized with the 06UTC GFS forecast fields.

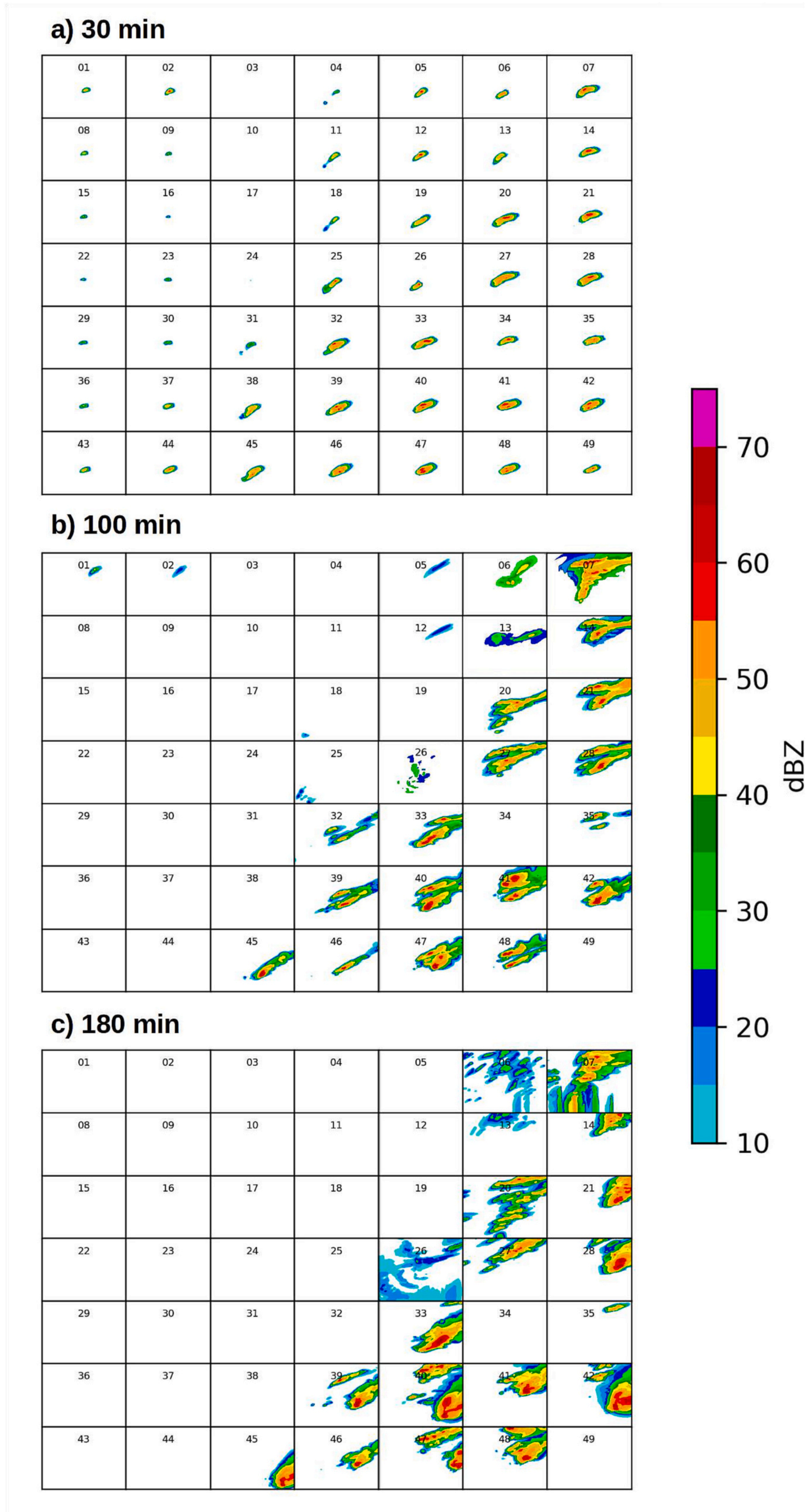

Fig. 9. As in Fig. 8 but for the simulations initialized with the 09UTC GFS forecast fields.

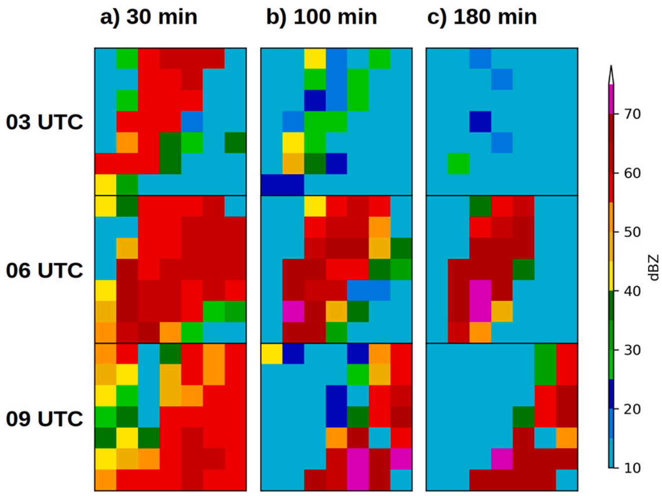

Fig. 10. The maximum spatial value of the reflectivity (dBZ) field for each CM1 simulation at the 30, 100 and 180 min simulation time outputs initialized at 03, 06 and 09 UTC 29 August 2020. The geographic location of each simulation within the 7x7 matrix corresponds to the same location as in Fig. 1.

agreement with the large scale analysis of the event. In the 03 UTC runs the developed supercells are short lived because they do not find a proper environment. None of them develops over land. The 06 UTC runs capture better the location (over the coast of Mallorca) as well as severity, but the 09 UTC runs are the more accurate representations as intense supercells develop mostly over the coast and land. Since the actual storm reached Mallorca at 9:30 UTC and these three sets of runs are initialized with the 29 August 2020 00UTC GFS run, in a operational context there would be at least a 9 h window to complete the simulations, examine the results and issue a warning if needed.

Fig. 11 shows equivalent computations but for the total accumulated rainfall. The rainfall pattern follows closely the evolution of the maximum reflectivity seen in Fig. 10. At the middle time of the simulations (100 min) rainfall values exceed 50 mm for many pseudo-soundings of the 06 and 09 UTC experiments and can be as large as 120 and 150 mm in some particular cases. By the end of the simulations (180 min) values over 80 mm are found at about half of the matrix cells. These high values of total rainfall agree with observations of the event as well as with the geographical location of the affected areas.

The matrix cell computations are finally repeated for the surface wind speed. Fig. 12 displays cell-maximum wind values over 20 m s^{-1}

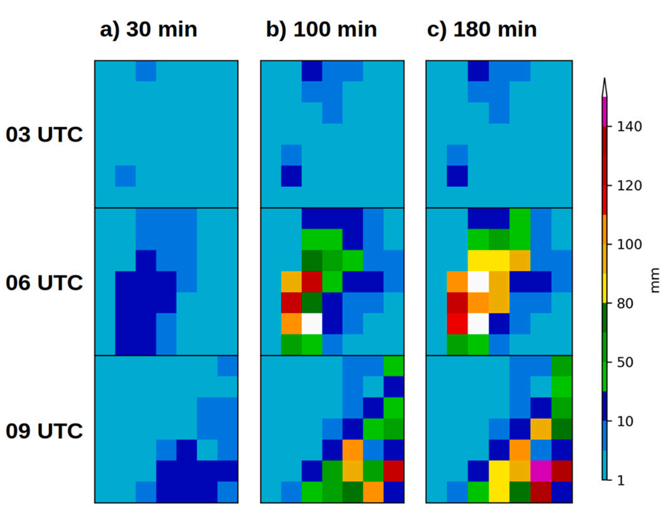

Fig. 11. As in Fig. 10 but for the maximum spatial value of total accumulated rainfall (mm).

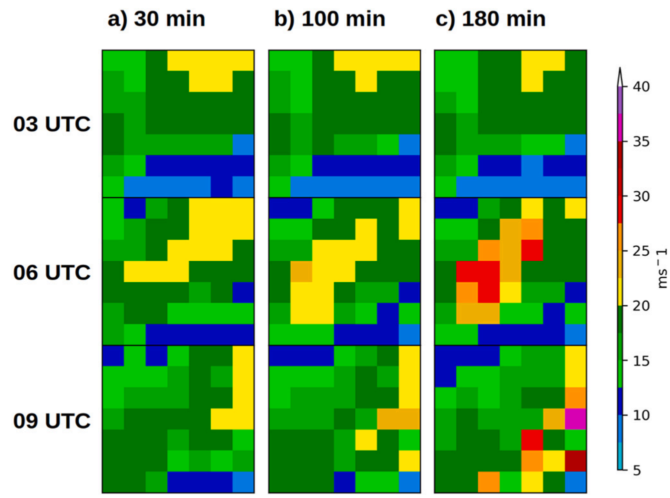

Fig. 12. As in Fig. 10 but for the maximum spatial value of surface wind (ms^{-1}).

following the convective storms, reaching higher values (up to 35 m s^{-1}) at the end of the simulations. Similarly to the rainfall field, the wind at surface follows the southeastwards migration and progressive enhancement of severe convective environments during the morning of 29 August. Accordingly, the highest values are found towards the southeast quadrant in the 06 UTC runs and neatly over this quadrant in the 09 UTC runs. The geographical location of extreme winds as well as the speed values themselves are in reasonable agreement with the location and intensity of the observed damaging winds. Existing records show winds of approximately 47 m s^{-1} (approximately 170 km h^{-1}) in the worst affected regions of Mallorca (*Valldemossa*, *Banyalbufar* and *Esporles* - near the southeast corner of the analysed matrix of environments).

4. Conclusions

The description and numerical analysis of the 29 August 2020 severe convective storm in Mallorca has been presented. The western coast of Mallorca was affected by extreme winds, hail and torrential rain. At least one EF2 category tornado affected the municipalities of *Valldemossa*, *Banyalbufar* and *Esporles*, producing vehicle traffic and power supplies interruptions. A supercell storm structure over the western Mediterranean was clearly caught by the radar images as it traveled eastwards, even showing a V-Notch feature when it crossed Mallorca.

The severe convective nature of the meteorological scenario is captured forehand by the GFS forecasts issued at 00 UTC 29 August 2020. The forecast fields valid at 03, 06 and 09 UTC exhibit high values of CAPE, SRH and EHI, compatible with the observed outcome of a supercell. However, these indicators alone do not provide final information on the effective likelihood of a supercell, its path or its severity. Therefore, a complementing strategy based on the use of the CM1 model has been proposed.

In essence, the region highlighted by classical analysis of convective potential is an ideal location for launching several CM1 runs to obtain more details on this convective potential and the attainable degree of severity. A square covering the targeted area with a sample of 49 CM1 simulations initialized at 03, 06 and 09 UTC from the 29 August 2020 00UTC GFS forecast fields have been considered. Each simulation is fed by a pseudo-radiosounding representing the environment and the results provide more useful information on the convective structures permitted by such environment. Since this strategy is applied to several locations and at several times, the results allow to effectively determine the spatial and temporal pattern of severe convective prone environments and how they evolve. Ad hoc indicators like maximum reflectivity or maximum surface wind speed can be examined to asses the degree of severity and hazardous potential.

The novel CM1-based approach presented here serves to further examine the convective potential of an environment as it couples application of a cloud model with the classic analysis of large scale ingredients. The goal is to provide better insights on the severity of a possible convective event already highlighted by the classic approach. A systematic -many simulations- approach like the one presented in this study is expensive computationally and this fact would prevent from an easy implementation for routine forecasting. However, a more targeted approach consisting of deploying fewer CM1 simulations would require lower computational resources and should be more than feasible. Running a few but representative CM1 simulations at strategic locations could allow forecasters to extract detailed information on the severity potential of a likely convective system, helping to issue more robust and reliable warnings.

CRediT authorship contribution statement

M. Vich: Methodology, Software, Validation, Formal analysis, Investigation, Resources, Data curation, Visualization, Writing – original draft, Writing – review & editing. **R. Romero:** Conceptualization, Methodology, Software, Validation, Investigation, Data curation, Supervision, Project administration, Funding acquisition, Writing – review & editing.

Declaration of Competing Interest

The authors declare that they have no known competing financial interests or personal relationships that could have appeared to influence the work reported in this paper.

Data availability

Data will be made available on request.

Acknowledgments

This work was sponsored by Spanish Ministerio de Ciencia e Innovación - Agencia Estatal de Investigación of Spain/TRAMPAS research project (PID2020-113036RB-I00/ AEI/ 10.13039/ 501100011033). We acknowledge George Bryan for freely providing the CM1 model and also the National Centers for Environmental Prediction for their open dissemination of the Global Forecast System (GFS) products used in this study.

References

AEMET, A.E.d.M., 2020a. Avance climatológico mensual Agosto 2020 en Illes Balears.http://www.aemet.es/documentos/es/serviciosclimaticos/vigilancia_clima/resumenes_climat/ccaa/illes-balears/avance_climat_bal_ago_2020.pdf. [Online; accessed 16-September-2022].
AEMET, A.E.d.M., 2020b. SINOBAS - SIstema de Notificación de OBservaciones Atmosféricas Singulares.https://sinobas.aemet.es/index.php?pag=detal&rep=1472. [Online; accessed 16-September-2022].
Bohren, C.F., Fraser, A.B., 1993. Green thunderstorms. Bull. Am. Meteorol. Soc. 74, 2185–2194.
Boyer, C.H., Dahl, J.M., 2020. The mechanisms responsible for large near-surface vertical vorticity within simulated supercells and quasi-linear storms. Mon. Weather Rev. 148, 4281–4297.
Bryan, G.H., 2008a. CM1 - Description of input sounding files.https://www2.mmm.ucar.edu/people/bryan/cm1/soundings/. [Online; accessed 3-September-2022].
Bryan, G.H., 2008b. CM1 homepage.https://www2.mmm.ucar.edu/people/bryan/cm1/. [Online; accessed 3-September-2022].
Bryan, G.H., Fritsch, J.M., 2002. A benchmark simulation for moist nonhydrostatic numerical models. Mon. Weather Rev. 130, 2917–2928.
Bunkers, M.J., Klimowski, B.A., Zeitler, J.W., Thompson, R.L., Weisman, M.L., 2000. Predicting supercell motion using a new hodograph technique. Weather Forecast. 15, 61–79.
Coffer, B.E., Parker, M.D., Thompson, R.L., Smith, B.T., Jewell, R.E., 2019. Using near-ground storm relative helicity in supercell tornado forecasting. Weather Forecast. 34, 1417–1435.
Deardorff, J.W., 1980. Stratocumulus-capped mixed layers derived from a three-dimensional model. Bound.-Layer Meteorol. 18, 495–527.
Ducrocq, V., Bougeault, P., 1995. Simulation of an observed squall line with a meso-beta-scale hydrostatic model. Weather Forecast. 10, 380–399.
Dudhia, J., 1993. A nonhydrostatic version of the penn state–ncar mesoscale model: Validation tests and simulation of an atlantic cyclone and cold front. Mon. Weather Rev. 121, 1493–1513.
EC, E.C., 2013. Enhanced Fujita scale for wind damage.https://www.canada.ca/en/environment-climate-change/services/seasonal-weather-hazards/enhanced-fujita-scale-wind-damage.html. [Online; accessed 3-September-2022].
Gallagher III, F.W., Beasley, W.H., Bohren, C.F., 1996. Green thunderstorms observed. Bull. Am. Meteorol. Soc. 77, 2889–2898.
Gayà, M., 2011. Tornadoes and severe storms in spain. Atmos. Res. 100, 334–343.
Gaya, M., Homar, V., Romero, R., Ramis, C., 2001. Tornadoes and waterspouts in the balearic islands: phenomena and environment characterization. Atmos. Res. 56, 253–267.
Hart, J., Korotky, W., 1991. The sharp workstation v1. 50 users guide. NOAA/National Weather Service, pp. 30.
Homar, V., Gaya, M., Ramis, C., 2001. A synoptic and mesoscale diagnosis of a tornado outbreak in the balearic islands. Atmos. Res. 56, 31–55.
Jo, E., Lasher-Trapp, S., 2022. Entrainment in a simulated supercell thunderstorm. part ii: The influence of vertical wind shear and general effects upon precipitation. J. Atmos. Sci. 79, 1429–1443.
Markowski, P.M., Dotzek, N., 2011. A numerical study of the effects of orography on supercells. Atmos. Res. 100, 457–478.
Markowski, P.M., Richardson, Y.P., 2014. The influence of environmental low-level shear and cold pools on tornadogenesis: Insights from idealized simulations. J. Atmos. Sci. 71, 243–275.
Meukaleuni, C., Lenouo, A., Monkam, D., 2016. Climatology of convective available potential energy (cape) in era-interim reanalysis over west africa. Atmos. Sci. Lett. 17, 65–70.
Morrison, H., Curry, J., Khvorostyanov, V., 2005. A new double-moment microphysics parameterization for application in cloud and climate models. part i: Description. J. Atmos. Sci. 62, 1665–1677.
Morrison, H., Curry, J., Shupe, M., Zuidema, P., 2005. A new double-moment microphysics parameterization for application in cloud and climate models. part ii: Single-column modeling of arctic clouds. J. Atmos. Sci. 62, 1678–1693.
Orf, L., Wilhelmson, R., Lee, B., Finley, C., Houston, A., 2017. Evolution of a long-track violent tornado within a simulated supercell. Bull. Am. Meteorol. Soc. 98, 45–68.
Patra, M., Louis, W.T.L., Kieu, C., 2022. Sensitivity of tropical cyclone intensity variability to different stochastic parameterization methods. Front. Earth Sci. 820.
Peters, J.M., Morrison, H., Nowotarski, C.J., Mulholland, J.P., Thompson, R.L., 2020. A formula for the maximum vertical velocity in supercell updrafts. J. Atmos. Sci. 77, 3747–3757.
Ramis, C., Arús, J., López, J.M., Mestres, A.M., 1997. Two cases of severe weather in catalonia (spain): an observational study. Meteorol. Appl. 4, 207–217.
Ramis, C., López, J.M., Arús, J., 1999. Two cases of severe weather in catalonia (spain). a diagnostic study. Meteorol. Appl. 6, 11–27.
Ramis, C., Romero, R., Homar, V., 2009. The severe thunderstorm of 4 october 2007 in mallorca: an observational study. Nat. Hazards Earth Syst. Sci. 9, 1237–1245.
Rasmussen, E.N., 2003. Refined supercell and tornado forecast parameters. Weather Forecast. 18, 530–535.
Romero, R., 2020. TRAM/ MeteoUIB homepage.https://meteo.uib.es/tram/. [Online; accessed 3-September-2022].
Romero, R., Ramis, C., Homar, V., 2015. On the severe convective storm of 29 october 2013 in the balearic islands: observational and numerical study. Q. J. R. Meteorol. Soc. 141, 1208–1222.
Romero, R., Vich, M., Ramis, C., 2019. A pragmatic approach for the numerical prediction of meteotsunamis in ciutadella harbour (balearic islands). Ocean Model. 142, 101441.
Sánchez, J., Fernández, M., Fernández, J., Tuduri, E., Ramis, C., 2003. Analysis of mesoscale convective systems with hail precipitation. Atmos. Res. 67, 573–588.
Schueth, A., Weiss, C., Dahl, J.M., 2021. Comparing observations and simulations of the streamwise vorticity current and the forward-flank convergence boundary in a supercell storm. Mon. Weather Rev. 149, 1651–1671.
Skamarock, W.C., Klemp, J.B., Dudhia, J., Gill, D.O., Liu, Z., Berner, J., Wang, W., Powers, J.G., Duda, M.G., Barker, D.M., et al., 2019. A description of the advanced research wrf model version 4. National Center for Atmospheric Research, Boulder, CO, USA, pp. 145.
SPC, S.P.C.R.T., 2007. The Enhanced Fujita Scale (EF Scale).https://www.spc.noaa.gov/efscale/. [Online; accessed 3-September-2022].
SPC, S.P.C.R.T., 2022. EXPLANATION OF SPC SEVERE WEATHER PARAMETERS. https://www.spc.noaa.gov/exper/mesoanalysis/help/begin.html. [Online; accessed 3-September-2022].
Spiridonov, V., Ćurić, M., Velinov, G., Jakimovski, B., 2021. Numerical simulation of a violent supercell tornado over vienna airport initialized and initiated with a cloud model. Atmos. Res. 261, 105758.
Taszarek, M., Allen, J.T., Brooks, H.E., Pilguj, N., Czernecki, B., 2021. Differing trends in united states and european severe thunderstorm environments in a warming climate. Bull. Am. Meteorol. Soc. 102, E296–E322.
Thompson, R.L., Edwards, R., Hart, J.A., Elmore, K.L., Markowski, P., 2003. Close proximity soundings within supercell environments obtained from the rapid update cycle. Weather Forecast. 18, 1243–1261.

Tudurí, E., Ramis, C., 1997. The environments of significant convective events in the western mediterranean. Weather Forecast. 12, 294–306.
Wade, A.R., Parker, M.D., 2021. Dynamics of simulated high-shear, low-cape supercells. J. Atmos. Sci. 78, 1389–1410.
Wang, P.K., 2002. The kansas green thunderstorm of 4 october 1998. Bull. Am. Meteorol. Soc. 83, 355–357.
Weisman, M.L., Klemp, J.B., 1982. The dependence of numerically simulated convective storms on vertical wind shear and buoyancy. Mon. Weather Rev. 110, 504–520.
Wicker, L.J., Skamarock, W.C., 2002. Time-splitting methods for elastic models using forward time schemes. Mon. Weather Rev. 130, 2088–2097.